Chemical Engineering Journal 315 (2017) 177–190

Contents lists available at ScienceDirect

Chemical Engineering Journal

journal homepage: www.elsevier.com/locate/cej

Synthesis of RGD-peptide modified poly(ester-urethane) urea electrospun nanofibers as a potential application for vascular tissue engineering

Tonghe Zhu [a], Kui Yu [a,c], M. Aqeel Bhutto [a], Xuran Guo [a], Wei Shen [a], Juan Wang [a], Weiming Chen [a], Hany El-Hamshary [d,e], Salem S. Al-Deyab [d], Xiumei Mo [a,b,*]

[a] State Key Laboratory for Modification of Chemical Fibers and Polymer Materials, College of Chemistry, Chemical Engineering and Biotechnology, Donghua University, Shanghai 201620, People's Republic of China
[b] Shandong International Biotechnology Park Development Co., Ltd., Yantai 264003, People's Republic of China
[c] College of Materials Science and Engineering, Donghua University, Shanghai 201620, People's Republic of China
[d] Department of Chemistry, College of Science, King Saud University, Riyadh 11451, Saudi Arabia
[e] Department of Chemistry, Faculty of Science, Tanta University, Tanta 31527, Egypt

HIGHLIGHTS

- A novel PEUU-RGD electrospun mats for vascular application were fabricated.
- PEUU-RGD mat was a good intima for prevent the formation of thrombi or hyperplasia.
- The fabricated mats showed excellent mechanical properties and high biocompatibility.
- Inhibition of platelet adhesion of the mats were also tuned.

ARTICLE INFO

Article history:
Received 22 July 2016
Received in revised form 29 December 2016
Accepted 31 December 2016
Available online 3 January 2017

Keywords:
Poly(ester-urethane) urea
Acrylamide-terminated glycine-arginine-glycine-aspartic peptides
Nanofibers
Covalent immobilization
Tissue engineering

ABSTRACT

The development of a biomimetic surface which is able to promote endothelialization is fundamental in the research for blood vessel substitutes to overcome the formation of thrombi or hyperplasia. In the present work, the fabrication of acrylamide-terminated glycine-arginine-glycine-aspartic peptides (Ac-GRGD) modified poly(ester-urethane) urea (PEUU) nanofibrous mats via electrospinning technique followed by covalent immobilizing method for improving its endothelialization was successfully achieved. Series of PEUU based polymers including PEUU, PEUU with t-butoxycarbonyl group (PEUU-Boc), and PEUU-amino group (PEUU-NH_2) were synthesized by a two-step solution polymerization and a de-protection process. The PEUU-RGD as-prepared nanofibrous mat was characterized using different techniques, such as, scanning electron microscopy, solide-state ^{13}C CP-MAS nuclear magnetic resonance, and stress-strain test. In addition, to motivate cell adhesion and proliferation, PEUU nanofibers mat was immobilized by coupling of Ac-GRGD. The results present that incorporation of Ac-GRGD peptide improved the mechanical properties and does not have negative effect on the morphology and the structure of PEUU nanofibers. From cell viability and cell morphology results, the prepared PEUU-RGD nanofiber mats are cytocompatible. Interestingly, the immobilized PEUU-RGD nanofibers possess lower hemolysis rate and an improved inhibition of platelet adhesion. Overall, Ac-GRGD peptides immobilized PEUU nanofibrous mats may have a potential application for vascular tissue engineering.

© 2017 Elsevier B.V. All rights reserved.

1. Introduction

For blood vessel tissue engineering, an ideal vascular replacement should possess excellent biocompatibility and mechanical properties [1,2]. It is also well known that native blood vessels consist of three different layers: intima, media, and adventitia. The intima, consists of a continuous monolayer of endothelial cells

* Corresponding author at: State Key Laboratory for Modification of Chemical Fibers and Polymer Materials, College of Chemistry, Chemical Engineering and Biotechnology, Donghua University, Shanghai 201620, People's Republic of China.
E-mail address: xmm@dhu.edu.cn (X. Mo).

http://dx.doi.org/10.1016/j.cej.2016.12.134
1385-8947/© 2017 Elsevier B.V. All rights reserved.

(ECs) [3]. A healthy endothelial layer is the only fully blood compatible surface that completely avoids thrombus development [4–6]. However, clinically employed vascular scaffolds do not spontaneously endothelialize; endothelial cells typically cover only a small percentage of the luminal surface, leaving a portion of the scaffolds without a complete endothelial cell layer [7,8]. However, tissue engineering offers a potential "ideal" small diameter vascular replacement with one concept creating biodegradable polymeric structures that would be used to provide mechanical support and continuous blood supply while promoting vascular tissue development in situ [9–12]. For this reason, how to promote endothelial cell growth, adhesion and proliferation on vascular scaffolds are an active area of research [13–15].

Electrospinning is a versatile technique, which can produce fibrous scaffolds with fiber diameters ranging from tens of nanometers to a few micrometers [16–18]. This method has been widely used to prepare tubular scaffolds with a rotation mandrel to collect the fibers [19]. The fibrous structures produced by the electrospinning could mimic the natural extracellular matrix (ECM) and contribute to the cell proliferation process by the electrospinning could mimic the natural extracellular matrix (ECM) and contribute to the cell proliferation process [20–24].

Segmented polyurethanes have been employed as elastomeric biomaterials because of their tunable mechanical properties, processability, and good biocompatibility in a variety of applications [25–27]. Although our group previous studies have shown that a novel method to developed PEUU based scaffold for the subsequent non-interfering modification with heparin and TPS peptide, but the patency of 20% at 8 weeks after implanted in rabbit carotid artery [28,29]. In this paper, the biodegradable PEUU-NH_2 elastomers were synthesized by a de-protection process from PEUU-Boc polymers. PEUU-NH_2 nanofibers immobilized with Ac-GRGD peptides were fabricated through carboxyl-amino condensation reaction. Additionally, in vitro assays with endothelial cells (human umbilical vein endothelial cells, HUVECs) were performed to test the potential of PEUU-RGD nanofibers to promote adhesion and control proliferation.

2. Materials and methods

2.1. Materials

Polycaprolactone diol (PCL2000, Mn = 2000), N-Boc-serinol (97%), hexamethylene dissocyanate (HDI), stannous octotate (Sn $(Oct)_2$), butanediamine were provided by Sigma-Aldrich and used as received unless specified. Acrylamido-terminated glycine-arginine-glycine-aspartic peptides (Ac-GRGD) and fluorescein isothiocyanate labeled acrylamido-terminated glycine-arginine-glycine-aspartic peptides (Ac-GRGD-FITC) were obtained from China Peptides Co., Ltd. (Shanghai, China). Chloroform (CF), trifluoroacetic acid (TFA), N-(3-dimethylaminopropyl)-N′-ethylcaobodiimide hydrochloride (EDC), and N-hydroxysuccinimide (NHS) were purchased from Sigma-Aldrich Trading Co., Ltd. (Shanghai, China). 1, 1, 1, 3, 3, 3-hexafluoro-2-propanol (HFIP) was acquired from Shanghai Darui Finechemical Co., Ltd. (Shanghai, China). Anhydrous ethanol (EtOH) and Anhydrous dimethylsulfoxide (DMSO) were purchased from Changshu Hongsheng Chemical Reagent Co., Ltd. (Changshu, China). Dulbecco's Modified Eagle's Medium (DMEM), fetal bovine serum (FBS), phosphate buffer saline (PBS, pH = 7.4), paraformaldehyde (POM), 3-(4, 5-Dimethylthiazol-2-yl)-2, 5-diphenyltetrazoliumbromide (MTT), penicillin–streptomycin and trypsin were purchased from Shanghai Yuanxiang Medical Equipment Co. Ltd (Shanghai, China). 4′, 6′-diamidino-2-phenylindole (DAPI) and rhodamine-conjugated phalloidin were obtained from Invitrogen (USA). All chemicals were used without further purification. Water used in all experiments was purified using a Milli-Q Plus 185 water purification system (Millipore, Bedford, MA) with resistivity higher than 18 MΩ cm.

2.2. Synthesis of PEUU based polymer

PCL diol (PCL2000) and N-Boc-serinol were dissolved in DMSO in a three-necked flask with the concentration of 10% (w/v) and HDI was added under nitrogen gas for protection. Followed this process, the addition of $Sn(Oct)_2$ (0.05 wt% based on the monomer concentration) and the reaction was carried out for 3 h at 80 °C. Butanediamine/DMSO solution at 2% (w/v) was added drop wise to the pre-polymer solution and the molar ratio of PCL2000 with N-Boc-serinol, HDI and butanediamine was 1:2:1. The reaction continued with stirring for 18 h at 40 °C. Then the polymer solution was extruded into the deionized water for precipitation. PEUU-Boc was eventually obtained after being dried in a vacuum oven at 60 °C for 48 h. PEUU was also synthesized in a similar method with the exceptional of addition N-Boc-serinol.

The synthesized PEUU-Boc was dissolved in CF/TFA solvent (v: v = 50/50) at the concentration of 5% (w/v, PEUU-Boc/solvent) in a round bottom flask and stirred for 1 h at 25 °C to remove the Boc-preotcted groups. The excess CF and TFA were moved by rotary evaporation and the polymer was precipitated and neutralized in 2% (w/v) Na_2CO_3 aqueous solution (pH = 11.4) to remove residual TFA. The product was then washed with distilled water and rinsed in isopropanol for 1 day, followed by drying in a vacuum oven at 60 °C for 2 days [29].

2.3. Fabrication of electrospun nanofibers

1.2 g of polymers (PEUU, PEUU-Boc, PEUU-NH_2) were dissolved in 10 mL of HFIP at room temperature for 24 h with vigorous magnetic stirring to prepare the solution for electrospinning.

The polymers (PEUU, PEUU-Boc, PEUU-NH_2) in 1, 1, 1, 3, 3, 3-hexafluoro-2-propanol (HFIP) solution (12%, w/v) were fed at 1.0 mL/h, 0.5 mL/h, 0.55 mL/h from a capillary charged at 9 kV, 10 kV, 8.45 kV, respectively, and perpendicularly located 14 cm from the target thin aluminum foil which acting as a collector which was positioned horizontally and grounded. All of the electrospinning processes were carried out at around 25 °C and 50% ± 2% relative humidity.

2.4. Nanofibers surface immobilization with Ac-GRGD peptide

Ac-GRGD molecules were covalently attached to the PEUU-NH_2 nanofibrous mats using EDC/NHS chemistry as previously described with modification [30]. Briefly, the PEUU-NH_2 nanofibrous mats were saturated with EtOH for 5 h prior to immobilization reaction. After this step, the PEUU-NH_2 nanofibrous mats were collected and washed first with PBS 3 time. At the same time, Ac-GRGD (8.98 mmol, 4 mg), EDC (100 mmol, 19.17 mg), and NHS (250 mmol, 28.77 mg) were dissolved in 2 mL DMSO, 2 mL PBS, 2 mL PBS, respectively. Then all the three solutions were mixed and stirred for 3 h to activate the carboxyl group of Ac-GRGD. The activated Ac-GRGD was added dropwise into the above PBS solution of the PEUU-NH_2 nanofibrous mats (10 mL) under stirring for 2 days. After 2 days crosslinking reaction at room temperature, mats were washed with copious amounts of distilled water to remove the byproducts, and then were lyophilized for 2 days. For comparison, PEUU-NH_2 with Ac-GRGD-FITC conjugation was also prepared in a manner similar to that used to form the PEUU-RGD-FITC nanofibrous mats. The only difference is the use of Ac-GRGD-FITC instead of the use of Ac-GRGD (Fig. 1(c)).

2.5. Nanofibrous mats characterizations

The morphology of the electrospun nanofibers were investigated by scanning electron microscopy (SEM) (JEOL, JSM-5600, Japan) at an accelerated voltage of 10 kV after sputter-coating with gold. The average fiber diameter was determined from 100 random measurements on a typical SEM image under lower magnification (1000×) using Image analysis software (Image-J, National Institutes of Health, USA). The contact angle was measured three times for each sample using a contact angle instrument (OCA40, Dataphysics, Germany) when the droplet was stable at 25 °C ± 0.5 °C and for a relative humidity of 30% ± 2%. The porosity of different nanofibers was measured using a method reported in the literature [31]. Three small strips (10 mm × 30 mm) were cut randomly from the nanofibrous mats. The thickness of the nanofibrous mats was measured with a micrometer and the apparent density (ρ_a) and porosity (p) were calculated from Eqs. (1) and (2), respectively.

$$\rho_a\ (\mathrm{g/cm^3}) = \frac{m\ (\mathrm{g})}{d\ (\mathrm{cm}) \times s\ (\mathrm{cm^2})} \tag{1}$$

$$p = \left(1 - \frac{\rho_a\ (\mathrm{g/cm^3})}{\rho_b\ (\mathrm{g/cm^3})}\right) \times 100\% \tag{2}$$

where m, d, and s stand for mass, thickness, and area of the strips, respectively. The bulk density (ρ_b) of PEUU is 1.16 g/cm^3.

Nanofibers was characterized by solide-state ^{13}C CP-MAS nuclear magnetic resonance (AVANCE-400, Bruker, Switzerland) with a ^{13}C resonance frequency of 100 MHz, contact time of 1.0 ms, and pulse delay time of 4.0 s. Fourier transform infrared (FTIR) spectra were recorded by absorption mode at 2 cm^{-1} interval in the range of 4000–600 cm^{-1} wave numbers, using a FT-IR spectrophotometer (Avatar380, USA). Wide-angle X-ray diffraction (WAXRD) curves were obtained on a D/max-2550 PC X-ray diffractometer (Rigaku Co., Tokyo, Japan) within the scanning region of 2θ (5–60°), with Cu Kα radiation (l = 1.5418 Å) at 40 kV and 40 mA. The fluorescent image of PEUU-RGD-FITC nanofibers was observed by a fluorescence microscope (Nikon TS100, Japan). For analysis, the nanofibers were loaded onto the glass slide during the process of electrospinning [32].

Thermal properties were measured by using a STAPT-1000 instrument (Linseis, German). Samples (3–5 mg) were heated from 29 °C to 600 °C at a heating rate of 10 °C/min under a flow of nitrogen (40 mL/min). The mechanical properties of nanofibrous mats were tested by a material testing machine (H5 K-S, Hounsfield, UK) with a crosshead speed of 10 mm/min under a load of 10 N, according to ASTM D638-98 (n = 5). All the nanofibrous mats were cut into small strips with the width × gauge length = 10 × 30 mm, and three strips from different sites of each fibrous mats sample were chosen for the tensile test. The stress and strain data were calculated using Eqs. (3) and (4) [3,33,34]:

$$\sigma\ (\mathrm{MPa}) = \frac{P\ (\mathrm{N})}{w\ (\mathrm{mm}) \times d\ (\mathrm{mm})} \tag{3}$$

$$\varepsilon = \frac{l}{l_0} \times 100\% \tag{4}$$

where σ, ε, *P*, *w*, *d*, *l*, and l_0 stand for stress, strain, load, mat width, mat length, extension length, and gauge length, respectively. Tensile strength, elongation at break, and Young's modulus were obtained from the strain-stress curves.

2.6. In vitro cell culture: cell viability and morphology of HUVECs cultured on the mats

HUVECs was cultured in Dulbecco's modified Eagle's medium (DMEM) with 10% fetal bovine serum and 1% antibiotic-antimycotic in an atmosphere of 5% CO_2 and 37 °C, and the medium was replenished every two days. All electrospun mats samples were placed into 24-well plates individually and secured by stainless rings. Before cell seeding, the nanofibrous mats were disinfected with 70% ethanol immersion for 12 h, followed washed 3 times with phosphate buffer solution (PBS), and then washed once again with culture medium [35]. For cell adhesion test, HUVECs were both seeded with a density of 1.0×10^4 cells/well. For cell proliferation test, HUVECs were seeded with a density of 8.0×10^3 cells/well.

MTT assay and SEM observation were employed to evaluate the viability and morphology of the adhered and proliferated HUVECs cultured onto different nanofibrous mats (n = 3 for each group) according to the manufacturer's protocol, respectively [36,37]. On a separate set of sheets, the attached cells were fixed with 4% paraformaldehyde and then 4′, 6′-diamidino-2-phenylindole hydrochloride (DAPI, Invitrogen, USA) and rhodamine-conjugated phalloidin (Invitrogen, USA) were used to stain the nucleus and cytoskeletons of cells. Specimens were observed under TS100 fluorescence microscope (Nikon, Japan).

2.7. Hemolysis assays

Fresh New Zealand white rabbit blood containing 3.8% sodium citrate injection (sodium citrate to distilled water ratio, 3.8:100 w/v) for anticoagulant (the ratio of anticoagulant to blood is 1:9, v/v) prepared reference to previous literature. Healthy red blood cells (HRBCs) were obtained by a pre-treatment procedure according to the literature before hemolysis assay [38]. In brief, the HRBCs were obtained by centrifuging the fresh blood (1200 r/min for 10 min), followed by washing the precipitates with PBS for 5 times to completely remove the serum. The HRBCs were 10 times diluted with PBS before hemolysis assay. The diluted HRBCs (0.2 mL) mixed with PBS solution (10 mL) with a total volume of 10.2 mL were added into centrifugal tube with bottom covered with PEUU nanofibrous mats, PEUU-Boc nanofibrous mats, PEUU-NH_2 nanofibrous mats, and PEUU-RGD nanofibrous mats (3 cm × 1 cm), respectively. The diluted HRBCs (0.2 mL) were also, respectively, mixed with 10 mL water (as a positive control) and 10 mL PBS buffer (as a negative control) in centrifugal tube for comparison. After a gentle shaking, all samples were incubated at 37 °C for 2 h. Then all the HRBC suspensions were taken away carefully and were centrifuged at 2000 r/min for 5 min. The absorbance at 545 nm of the supernatant (hemoglobin) was determined by Lambda 25 UV–Vis spectrophotometer (Perkin Elmer, USA). Hemolysis rate (HR) was defined as follows:

$$\mathrm{HR} = \frac{\mathrm{SA} - \mathrm{NA}}{\mathrm{PA} - \mathrm{NA}} \times 100\% \tag{5}$$

where SA, PA, and NA stand for the absorbency of the experimental sample, the positive control and the negative control, respectively. Mean and standard deviation of the triplicate centrifugal tubes for each sample were calculated.

2.8. Platelet adhesion test

Rabbit platelet-rich plasma was obtained from healthy female New Zealand White rabbits in compliance with protocols approved by the Institutional Review Board for Human Investigations at the Shanghai Jiaotong University School of Medicine. Blood was drawn into plastic Vacutainer tubes containing 3.2% sodium citrate.

Platelet-rich plasma (PRP, 2×10^7 platelets/mL) was obtained by centrifugation at 1500 rpm for 10 min at room temperature.

All nanofibrous mats (PEUU nanfibrous mats, PEUU-Boc nanofibrous mats, PEUU-NH_2 nanofibrous mats, and PEUU-RGD nanofibrous mats; n = 3 for each group) with disk shapes (diameter = 15 mm) were placed into 24-well plates individually and secured by stainless rings. Then, disk samples were sterilized with 70% ethanol immersion for 2 h, and rinsed with deionized water three times. Finally, PRP (350 μL/well) were seeded on the samples [29].

After 3 h incubation at 37 °C with mild shaking, the samples were gently rinsed with deionized water to wash away nonattached platelets. Then, the platelets deposited on the surface were fixed in 4% paraformaldehyde, and dehydrated with gradient alcohol and dried at room temperature. Finally, the platelets adhered on nanofibrous mats were sputter-coated with gold for SEM observation. The number of adherent platelets was determined by detecting the activity of lactate dehydrogenase (LDH Release Assay Kit, Beyotime, Nantong, China) present after cell lysis as previously described [35].

2.9. Statistical analysis

In our all the experiments, all results are represented as the mean ± standard deviation (SD). The data were analyzed by one-way ANOVA, followed by Tukey's test for the evaluation of specific differences with Origin Pro 8.0 (Origin lab Inc., USA). A value of 0.05 was selected as the significance level, and the data were indicated with (*) for $p < 0.05$, (**) for $p < 0.01$, and (***) for $p < 0.001$, respectively [28,29].

3. Results and discussion

3.1. Fabrication and characterization of PEUU based nanofibers

3.1.1. Synthesis and chemical structure of PEUU based polymers

In the last decades a large number of synthetic polymers with various different properties are available for vascular tissue engineering applications. Most of the polymers have no sufficient mechanical stability and elasticity as well as inadequate interaction between polymer and cells. In this study, the PEUU based polymer was synthesized via a two-step solution polymerization method according to our previous work [28,29,35], whereas the main different is using butanediamine instead of putrescine, which was synthesized through isocyanato-amino or isocyanato-hydroxy condensation reaction, as shown in Fig. 1(a). Firstly, PCL2000-HDI and N-Boc-serinol-HDI conjugates were synthesized via an isocyanato-hydroxy condensation reaction between the hydroxyl groups of PCL2000 and the isocyanato groups of HDI or the hydroxyl groups of N-Boc-serinol and the isocyanato groups of

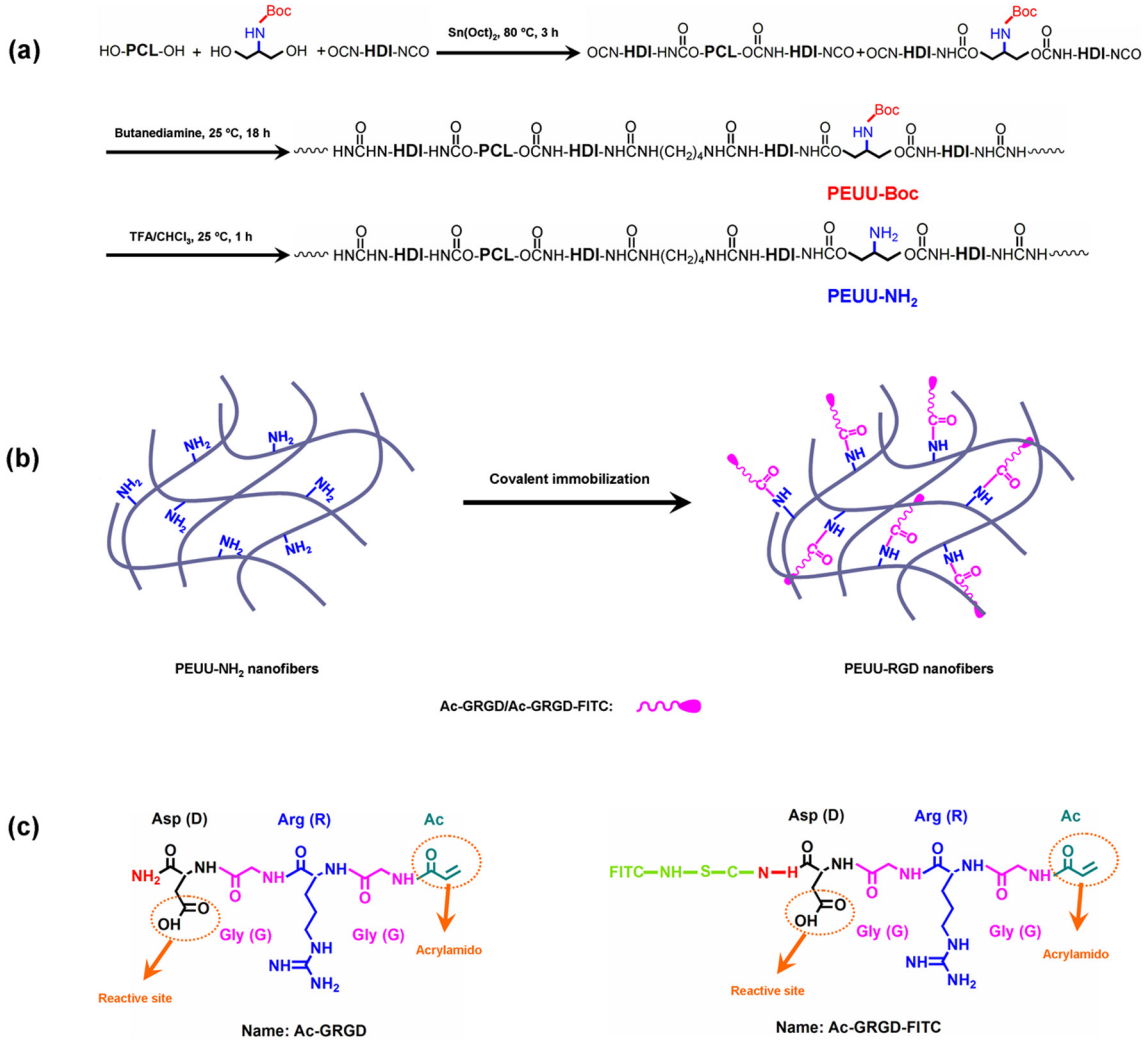

Fig. 1. Schematic illustration for synthesis of PEUU based polymers and the process of fabrication PEUU-RGD nanofibers.

HDI, respectively (the first step in Fig. 1(a)). Secondly, PCL2000-HDI and N-Boc-serinol-HDI was conjugated through isocyanato-amino condensation reaction between the amino groups of butanediamine and the isocyanato groups of PCL2000-HDI or N-Boc-serinol-HDI (the second step in Fig. 1(a)). Then after de-protection of the Boc groups, PEUU-NH_2 polymer was obtained (the third step in Fig. 1(a)). Fig. 1(b) shows the schematic representation for Ac-GRGD surface immobilization for PEUU-NH_2 nanofibrous mats by carboxy-amino condensation reaction (Fig. 1(b)). In order to prove Ac-GRGD peptides immobilized onto the surface of PEUU nanofibers, we also have used FITC conjugated Ac-GRGD which immobilized onto the surface of PEUU nanofibers instead of Ac-GRGD, as shown in Fig. 1(c).

Chemical structures of different nanofibers were qualitatively confirmed by FTIR spectroscopy. The spectrums presented in Fig. 2(a) show the characteristic peak of PEUU which are around 1725 cm^{-1} (ester carbonyl group), 1570 cm^{-1} (the deformation vibration in plane of N–H), the broad peak at 1161 cm^{-1} and 1236 cm^{-1} represent the stretching vibration of C–O–C. The peaks at 1454 cm^{-1} and 1088 cm^{-1} are attributed to the vibration of the C–N stretch and C–O stretch bonding, respectively. A few of the peaks magnitude have no significantly change when Ac-GRGD group were immobilized onto the nanofibers, likely due to the insensitivity of the FTIR technique.

The crystallinity of polymers was further confirmed by WAXRD (Fig. 2(b)). Peaks at $2\theta = 21.5°$ corresponded to the crystalline structure of the soft segment in PEUU. The crystalline peak of PEUU shows no significant difference before and after immobilized modified. Furthermore, Ac-GRGD peptides immobilized electrospun PEUU nanofibers only displayed a broad and diffuse diffraction peak at 2θ of 21.5°, which indicated that solvent (DMSO) have destroyed the crystal structure on the surface of PEUU-NH_2 in the process of covalent immobilization [35].

The ^{13}C CP/MAS NMR spectra of PEUU, PEUU-Boc, PEUU-NH_2, and PEUU-RGD electrospun nanofibers are shown in Fig. 2(c). The chemical shift assignments are list in Table 1. There exist two kinds of –NH groups in PEUU-based polymer: one is in the urethane unit and the other is in the urea unit. The ^{13}C peaks appearing at 170.0 ppm and 162.5 ppm are assigned to the carbonyl carbons in the urea and urethane groups, respectively. Other ^{13}C peaks as shown in Table 1. The ^{13}C peaks of PEUU, PEUU-Boc, PEUU-NH_2, and PEUU-RGD electrospun nanofibers have no significant different, this is because they have similar molecular backbones, as shown in Fig. 2(e).

Fluorescence microscopy was used to confirm the existence of Ac-GRGD onto PEUU nanofibers. The Ac-GRGD immobilized onto PEUU nanofibers can be clearly observed by the green fluorescence of Ac-GRGD-FITC using a fluorescence microscope (Fig. 2(d)). The Ac-GRGD peptide immobilized PEUU nanofibers exhibited a uniform green fluorescence, which is attributed to homogeneous immobilization of Ac-GRGD peptide onto the nanofibers. This result revealed that the Ac-GRGD peptide can be immobilized onto PEUU nanofibers with uniform distribution on the surface of PEUU nanofibers.

Table 1
Assignments of ^{13}C CP/MAS NMR chemical shifts of PEUU, PEUU-Boc, PEUU-NH_2, and PEUU-RGD electrospun nanofibers, where the structure of the repeat unit is shown in Fig. 2(e).

Chemical shift (ppm)	Assignment	Chemical shift (ppm)	Assignment
170.0	CO (urea)	24.5 ~ 32.5	C3 + C4 + C5
162.5	CO (urethane)	42.3	C2
62.5–69.5	C1	–	–

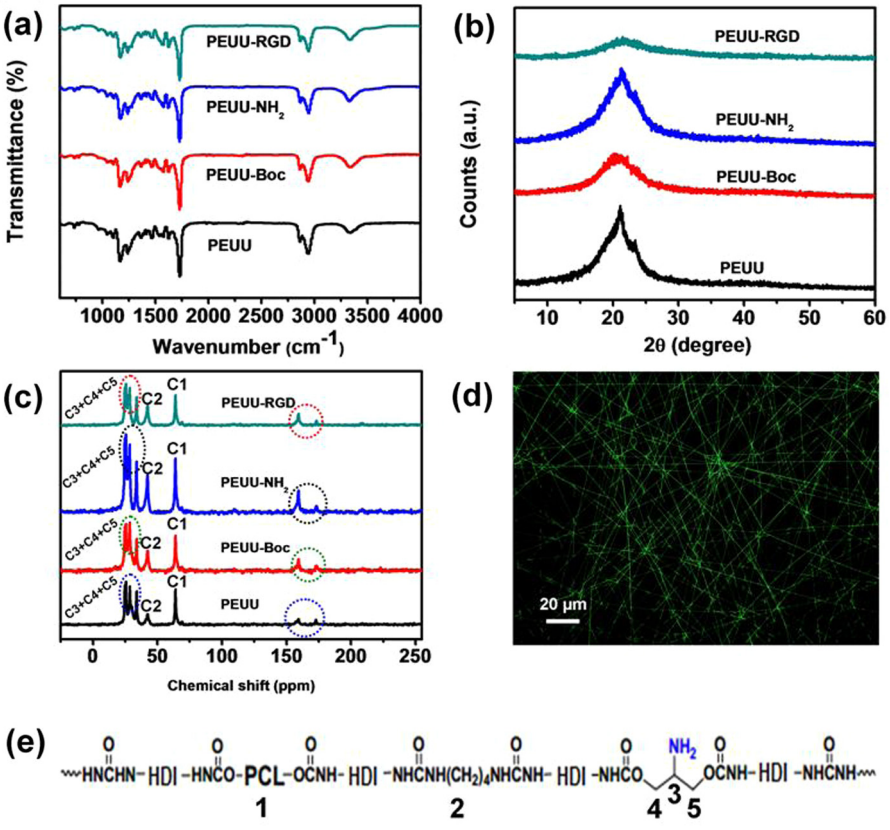

Fig. 2. (a) ATR-FTIR spectra, (b) X-ray diffraction pattern, and (c) ^{13}C CP/MAS NMR spectra of PEUU, PEUU-Boc, PEUU-NH_2, and PEUU-RGD electrospun nanofibers, respectively, and (d) fluorescent image of PEUU-RGD-FITC electrospun nanofibers and (e) the molecular backbone of PEUU based polymers.

3.1.2. Surface morphology and hydrophilicity of PEUU based nanofibers

The surface morphology and diameter distribution of the formed nanofibers were observed by SEM (Fig. 3). It can be seen that the surface of these nanofibers display a porous three-dimensional structure, and the diameter of these nanofibers keep a relatively narrow distribution range. In comparison to PEUU nanofibers and PEUU-NH_2 nanofibers, the fiber diameters decrease

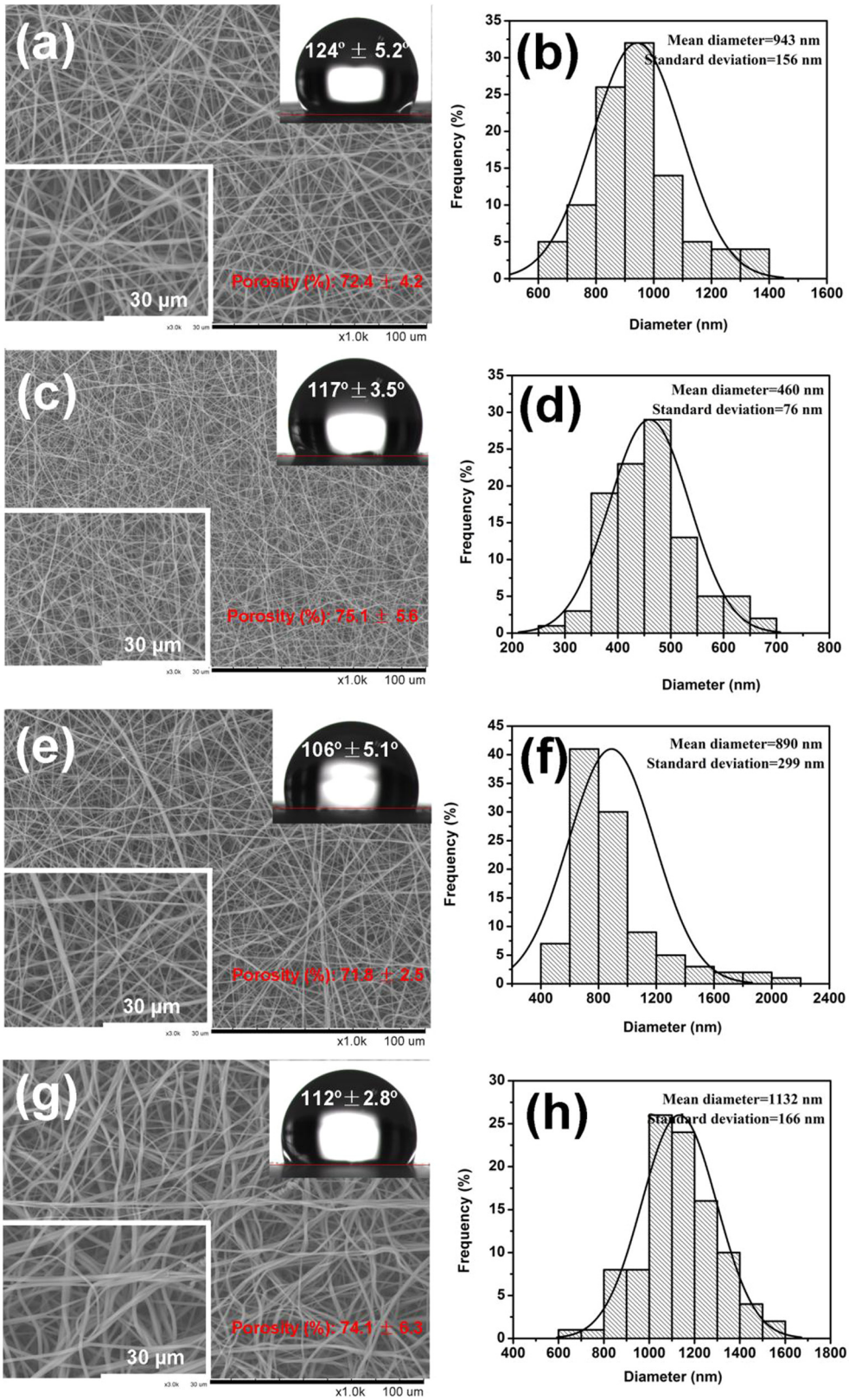

Fig. 3. SEM images, diameter distribution histograms, porosity and water contact angle of PEUU nanofibrous mats (a) and (b), PEUU-Boc nanofibrous mats (c) and (d), PEUU-NH_2 nanofibrous mats (e) and (f), PEUU-RGD nanofibrous mats (g) and (h).

of PEUU-Boc nanofibers are presumably due to the existence of t-butoxycarbonyl group, which was possess positive charge and enhanced the traction on the surface of droplet. Combining with Fig. 4 which is the corresponding representative mechanical property data of PEUU nanofibrous mats, PEUU-Boc nanofibrous mats, PEUU-NH_2 nanofibrous mats, and PEUU-RGD nanofibrous mats, the tensile strength of either PEUU nanofibrous mats or PEUU-RGD nanofibrous mats was increased compared with PEUU-Boc nanofibrous mats and PEUU-NH_2 nanofibrous mats. This is likely due to the diameter of PEUU nanofibers (943 nm) and PEUU-RGD nanofibers (1132 nm) are thicker than other two nanofibrers (460 and 890 nm). Porosity and surface hydrophilicity are important parameters for the electrospun nanofibers to be used in tissue engineering applications. The porosity and water contact angle data of PEUU nanofibrous, PEUU-Boc nanofibers, PEUU-NH_2 nanofibers, and PEUU-RGD nanofibers are also shown in Fig. 3. It is interesting that the anisotropy of water contact angles was shown on all the nanofibrous mats regardless of the surface chemistry difference, which could be due to the chemical groups (t-butoxycarbonyl group, amino, and Ac-GRGD peptides) on the surfaces of PEUU nanofibers does not seem to significantly alter the porosity and the hydrophilicity of PEUU nanofibers [39]. Furthermore, this might also be the reason that PEUU is a kind of hydrophobic polymer and the hydrophily of PEUU is hard to be changed by lower Ac-GRGD peptide surface density. In summary, the hydrophilicity of PEUU-Boc nanofibers can't be changed by the immobilization of Ac-GRGD peptide. Nevertheless, PEUU-RGD nanofibrous mats are most suitable as a scaffold because RGD groups have high affinity with the cells during cell growth. Therefore, PEUU-RGD nanofibrous mats can provide a good environment for cell attachment and proliferation [7,33,40].

3.2. Mechanical and thermal properties of nanofibrous mats

The representative tensile stress-strain curves and mechanical property data of PEUU nanofibrous mats, PEUU-Boc nanofibrous mats, PEUU-NH_2 nanofibrous mats and PEUU-RGD nanofibrous mats are shown in Fig. 4. Compared with PEUU nanofibrous mats, the tensile strength and elongation at break of PEUU-Boc nanofibrous mats, PEUU-NH_2 nanofibrous mats and PEUU-RGD nanofibrous mats were decreased, while the Young's modulus (the strain range as shown in Fig. 4(a) inset: PEUU nanofibrous mats 40–200%, PEUU-Boc nanofibrous mats 30–160%, PEUU-NH_2 nanofibrous mats 40–140% and PUU-RGD nanofibrous mats 40–170%) of both PEUU-Boc nanofibrous mats and PEUU-NH_2 nanofibrous mats were significantly increased (as show in Table 2 and Fig. 4(a)). The results suggested that the Ac-GRGD peptide covalent immobilized with amino onto PEUU-NH_2 can act as the physical crosslinker to form a stiff network on the nanofibers matrix and enhance the Young's modulus of PEUU-RGD nanofibers compared with PEUU-Boc nanofibrous mats and PEUU-NH_2 nanofibrous mats. Excessive interaction between groups, active group especially amino partially agglomerated and consequently formed stress concentration on nanofibers, as a result, the tensile strength of PEUU-Boc nanofibrous mats and PEUU-NH_2 nanofibrous mats decreased [41]. The decrease in the elongation at break of PEUU-NH_2 nanofibrous mats compared to PEUU nanofibrous mats may be due to the excessive interaction between amino and

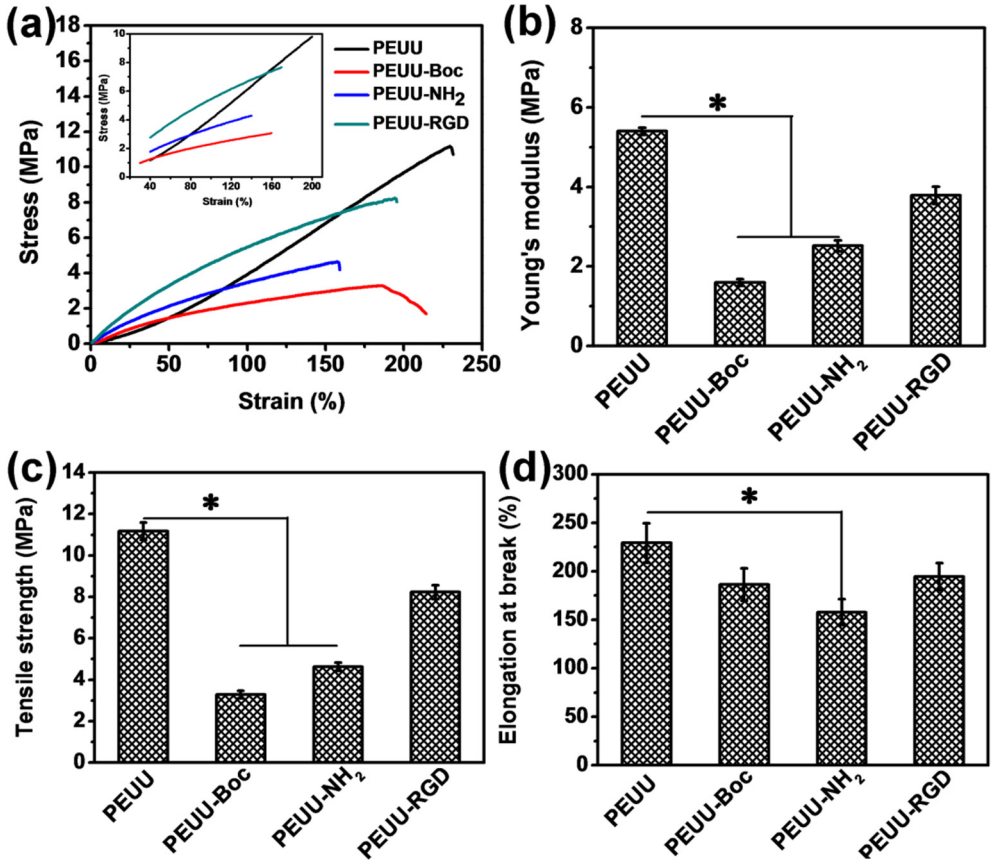

Fig. 4. Mechanical properties of PEUU nanofibrous mats, PEUU-Boc nanofibrous mats, PEUU-NH_2 nanofibrous mats and PEUU-RGD nanofibrous mats under dry conditions: (a) representative stress-strain curves, inset shows the magnification of calculating range of Young's modulus; (b) Young's modulus; (c) tensile strength; (d) elongation at break.

Table 2
Tensile properties of PEUU nanofibers, PEUU-Boc nanofibers, PEUU-NH_2 nanofibers, and PEUU-RGD nanofibers (data are representatives of independent experiments and all data are given as mean ± SD, n = 3).

Sample	Tensile strength (MPa)	Elongation at break (%)	Young's modulus (MPa)
PEUU	11.2 ± 0.4	229.2 ± 20.4	5.4 ± 0.1
PEUU-Boc	3.2 ± 0.2	186.4 ± 16.7	1.6 ± 0.1
PEUU-NH_2	4.6 ± 0.2	157.9 ± 13.3	2.5 ± 0.2
PEUU-RGD	8.2 ± 0.3	194.5 ± 14.1	3.8 ± 0.1

consequently formed stress concentration on nanofibers [42]. As the Ac-GRGD peptide immobilized PEUU molecular chains can mix and tightly entangle each other, the Ac-GRGD peptide are strongly tethered to PEUU nanofibers matrix. As a result, the tensile strength and elongation at break of PEUU-RGD nanofibrous mats and PEUU nanofibers are similar. On the other hand, the Young's modulus of PEUU-RGD nanofibrous mats was significantly higher than other specimens.

Thermogravimetric analysis is considered to be the most important method for studying the thermal stability of polymers. Fig. 5 shows the TG curves and DTG curves of PEUU nanofibrous mats, PEUU-Boc nanofibrous mats, PEUU-NH_2 nanofibrous mats and PEUU-RGD nanofibrous mats, respectively. A moderate decrease in weight before 100 °C could be due to the vaporization of water in nanofibrous mats. The weight decreased rapidly from approximately 200 °C to 500 °C, which can be attributed to the thermal decomposition of the main chain of PEUU based polymers. It can be seen that the onset temperature of thermal degradation of the four samples is between 265 °C and 275 °C, and the thermal degradation temperature of 50% weight loss is near 350 °C. Compared with the two pyrolytic process of PEUU nanofibrous mats, the pyrolytic process of PEUU-Boc nanofibrous mats, PEUU-NH_2 nanofibrous mats and PEUU-RGD nanofibrous mats possess three stages: the dehydration of polymers, thermal fracture of main molecular chains and thermal scission of side chains (active groups: t-butoxycarbonyl group, amino, or Ac-GRGD peptide). In addition, the thermal degradation temperature of 50% weight loss of PEUU-Boc nanofibrous mats, PEUU-NH_2 nanofibrous mats and PEUU-RGD nanofibrous mats both increased slightly. This may due to the interaction between active groups (t-butoxycarbonyl group, amino, or Ac-GRGD peptide) and consequently formed tightly entanglement of molecular chains. The peak decomposition temperature of the DTG curves represented the temperature at which the maximum weight loss rate is reached, as shown in Fig. 5(b). The peak decomposition temperature of PEUU nanofibrous mats appears about 325 °C and significantly less than the other three samples. From curves in Fig. 5(b), it can be observed that a diffuse peak appears about 440 °C on the curve of PEUU-Boc nanofibrous mats, PEUU-NH_2 nanofibrous mats and PEUU-RGD nanofibrous mats, respectively, which are attributed to the existence of side chains (active groups: t-butoxycarbonyl group, amino, or Ac-GRGD peptide). Therefore, the result proved that the Ac-GRGD peptide had been grafted onto PEUU nanofibers again.

3.3. Cytocompatibility assay

For further tissue engineering applications, it is important to ensure the biocompatibility of the developed nanofibrous mats. The intima for vascular scaffolds was typically designed to promote

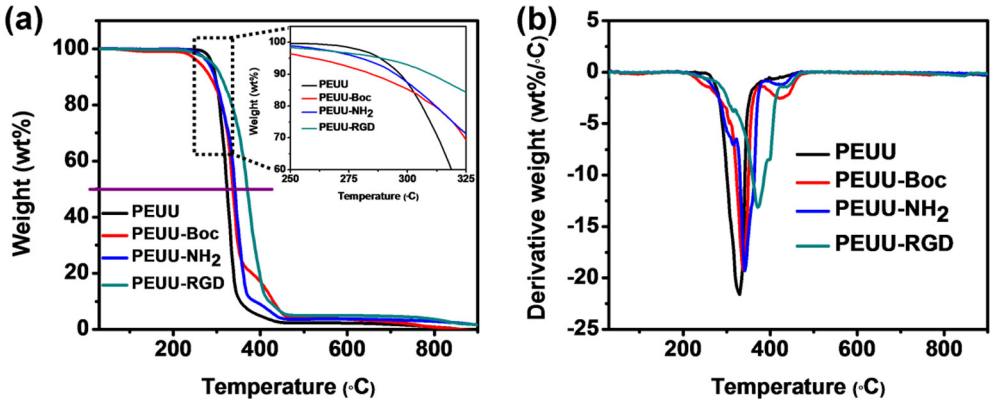

Fig. 5. TG curves (a) and DTG curves (b) of PEUU nanofibrous mats, PEUU-Boc nanofibrous mats, PEUU-NH_2 nanofibrous mats and PEUU-RGD nanofibrous mats.

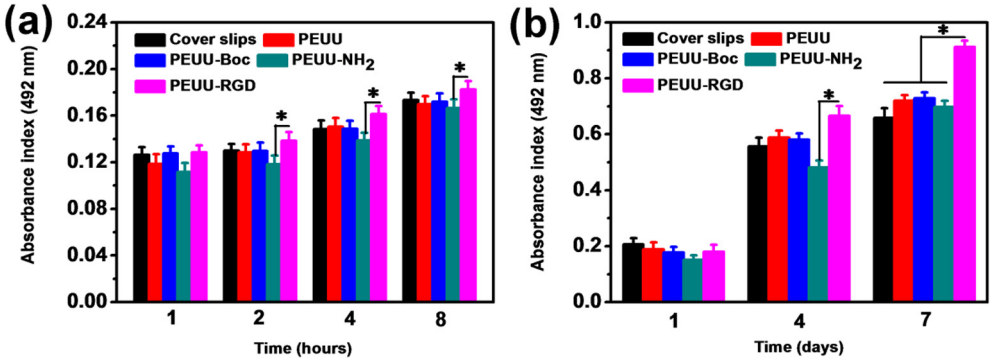

Fig. 6. MTT assay of the adhesion viability (a) and the proliferation viability (b) of HUVECs cultured onto cover slips, PEUU nanofibrous mats, PEUU-Boc nanofibrous mats, PEUU-NH_2 nanofibrous mats and PEUU-RGD nanofibrous mats, respectively.

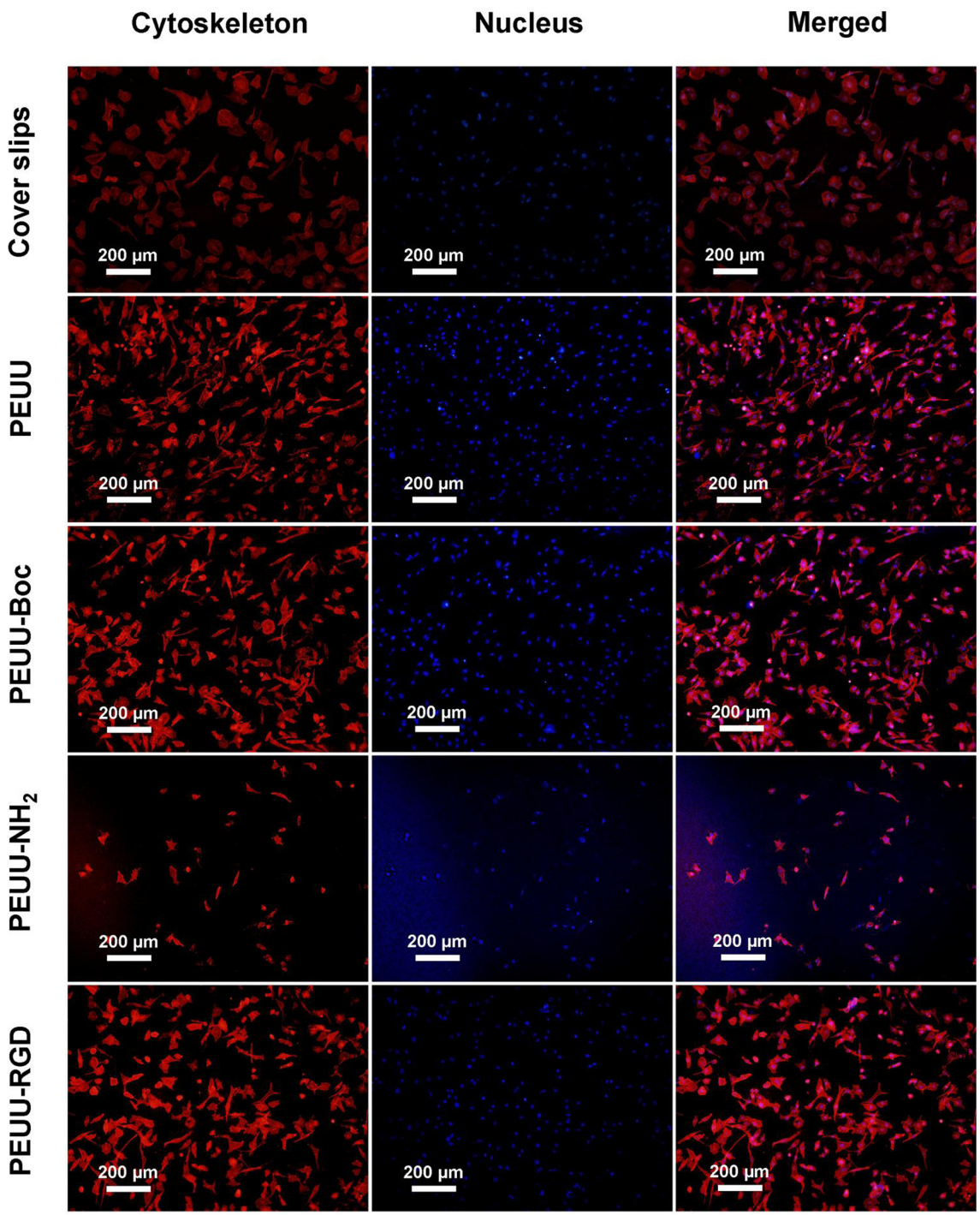

Fig. 7. Fluorescence microscopy images of HUVECs cultured onto cover slips, PEUU nanofibrous mats, PEUU-Boc nanofibrous mats, PEUU-NH_2 nanofibrous mats and PEUU-RGD nanofibrous mats with labeling of cytoskeleton (red) and nucleus (blue) after 8-h culture, respectively. (For interpretation of the references to color in this figure legend, the reader is referred to the web version of this article.)

endothelial cell growth, physiological functions, and maintain normal states of cell differentiation [37,43,44]. The HUVECs adhesion and proliferation were investigated to evaluate whether the PEUU-RGD nanofibrous mats satisfied the fundamental requirement in vascular tissue engineering. The adhesion behavior of HUVECs onto the nanofibrous mats was evaluated in 8 h (Fig. 6 (a)). Compared with cover slips group, HUVECs exhibited good adhesion to the PEUU-RGD nanofibrous mats. The biomimetic structure of nanofibrous mats and the capability of in situ regenerative of Ac-GRGD peptide which was immobilized onto the surface of electrospun poly(ester-urethane) urea polymer nanofibers afford the mats with better adhesion viability compared with the former reports [35,45].

The proliferation of HUVECs on days 1, 4, and 7 after cultured on nanofibrous mats is shown in Fig. 6(b). In addition to PEUU-NH_2 nanofibrous mats group the HUVECs cultured on the nanofibrous mats grew better than those cultured on cover slips on the fourth day, and especially on the seventh day. The viability of HUVECs cultured onto PEUU-NH_2 nanofibrous mats is much lower than other groups and this may due to the existence of amino which

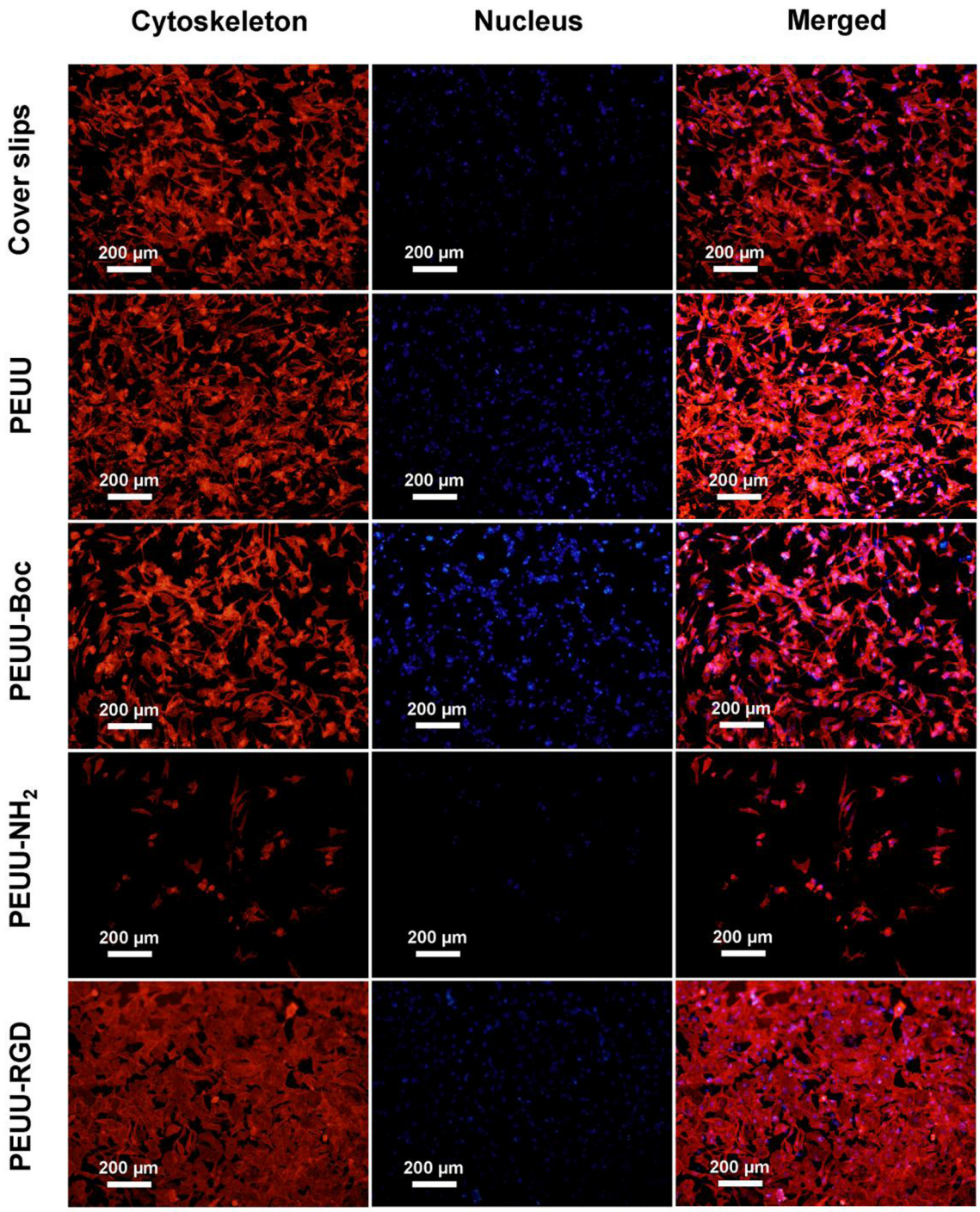

Fig. 8. Fluorescence microscopy images of HUVECs cultured onto cover slips, PEUU nanofibrous mats, PEUU-Boc nanofibrous mats, PEUU-NH_2 nanofibrous mats and PEUU-RGD nanofibrous mats with labeling of cytoskeleton (red) and nucleus (blue) after 4-day culture, respectively. (For interpretation of the references to color in this figure legend, the reader is referred to the web version of this article.)

provides an adverse alkaline environment for cells growth. After Ac-GRGD peptide was immobilized onto the surface of electrospun poly(ester-urethane) urea polymer nanofibers, the rate of cell proliferation increased dramatically. The result is in agreement with previous literature [35]. This implies that cells were specifically attached with the surface via Ac-GRGD-integrin receptor interactions. The obvious increment of cell proliferation rate also supports the specific interaction between cells and RGD moieties in Ac-GRGD.

The cytocompatibility of PEUU-RGD nanofibrous mats was further confirmed by observing the morphology of HUVECs cultured onto the nanofibrous mats after 8th hours and 4th days of incubation by rhodamine-conjugated phalloidin/DAPI staining via fluorescence microscopy, which expressed cell nucleus with blue color while fluorescence labeled cytoskeleton with red color (Figs. 7and 8). The density of HUVECs cultured on PEUU nanofibrous mats and PEUU-RGD nanofibrous mats were higher than cover slips, PEUU-Boc nanofibrous mats and PEUU-NH_2 nanofi-

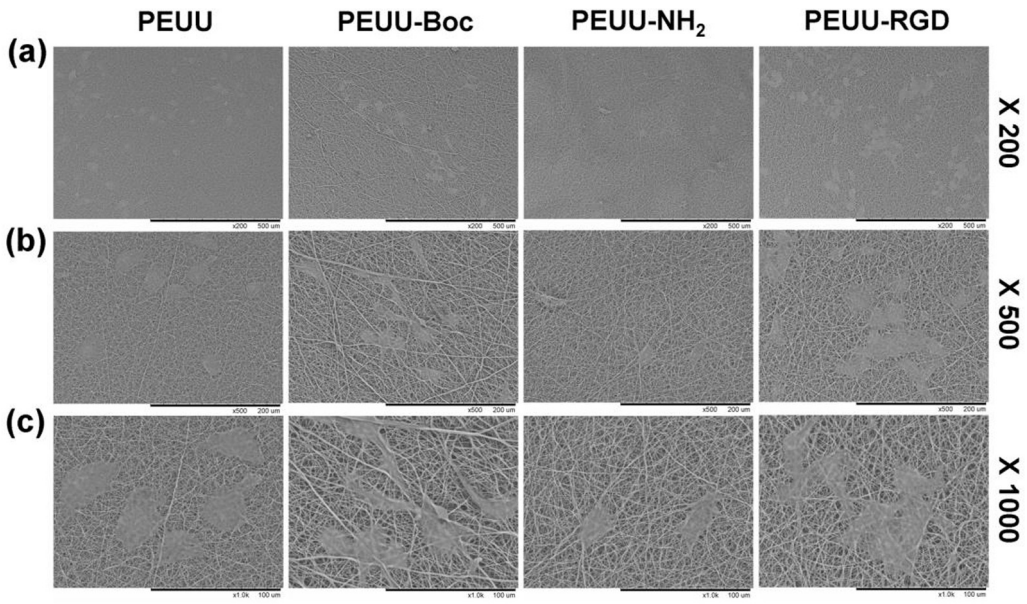

Fig. 9. SEM micrographs of HUVECs grown onto PEUU nanofibrous mats, PEUU-Boc nanofibrous mats, PEUU-NH_2 nanofibrous mats and PEUU-RGD nanofibrous mats after 4-day culture and (a) magnified 200 times, (b) magnified 500 times, (c) magnified 1000 times, respectively.

brous mats. This might due to two reasons, Firstly on the surface of Ac-GRGD peptide immobilized nanofibers the change in surface cytocompatibility property enhances the cell adhesion and proliferation rate and secondly the existence of t-butoxycarbonyl group or amino in the cell surrounding limit the HUVECs activity. The HUVECs morphology on nanofibrous mats were shown via SEM images (Fig. 9). It is also reveal the cell-cell and cell-matrix interaction. The results suggested that HUVECs cultured onto the PEUU-RGD nanofibrous mats more easily spread than those cultured onto PEUU nanofibrous mats, PEUU-Boc nanofibrous mats, PEUU-NH_2 nanofibrous mats. This observation also could be confirmed in Fig. 9 PEUU-RGD nanofibrous mats, where cells obviously formed spindle like or triangular shapes, indicating the suitable environment of PEUU-RGD nanofibrous mats for cell growth. These cells morphology observation data corroborate the results of MTT assay.

3.4. Hemocompatibility of nanofibrous mats

Hemolytic activity is one of the key indicators to evaluate the hemocompatibility of implant materials such as vascular replacements [46]. The release of adenosine diphosphate within the broken red blood cells can strengthen the assembly of blood platelets, which accelerates the formation of clotting and thrombus [47]. The hemolysis test results of PEUU nanofibrous mats, PEUU-Boc nanofibrous mats, PEUU-NH_2 nanofibrous mats and PEUU-RGD nanofibrous mats are also shown in Fig. 10. The hemolysis rate (HR) of PEUU-RGD nanofibrous mats is about 1.21%, which is far less than the value of safe limit (5%). On the other hand compared with PEUU nanofibrous mats and PEUU-NH_2 nanofibrous mats, PEUU-RGD nanofibrous mats exhibit much lower HR.

SEM images showed platelets adhesion on surfaces of nanofibrous mats following 3 h incubation of rabbit platelet-rich plasma (Fig. 11(a)–(d)). A large number of platelets deposited onto PEUU nanofibrous mats and PEUU-NH_2 nanofibrous mats with some of the deposited platelets extending pseudopodia. In contrast, platelet deposition onto PEUU-RGD nanofibrous mats was markedly reduced (Fig. 11), with sparse deposition of individual platelets observed. Quantification of platelet deposition using the LDH assay (Fig. 11(e)) confirmed the visual results, with PEUU-RGD nanofibrous mats exhibiting significantly lower platelet deposition than

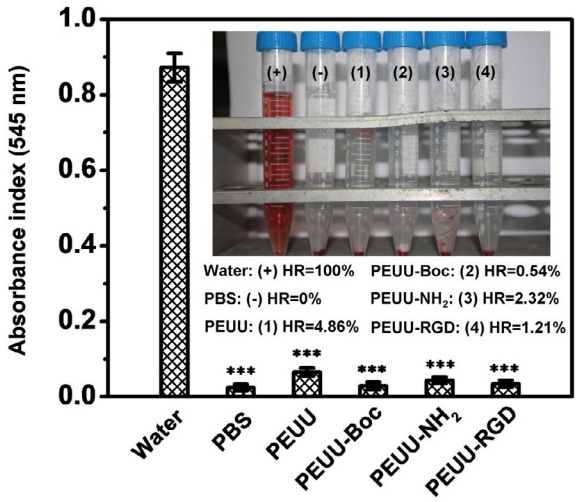

Fig. 10. Hemolytic assay of electrospun PEUU (1), PEUU-Boc (2), PEUU-NH_2 (3), and PEUU-RGD (4) nanofibrous mats. Water (+) and PBS (−) was used as positive and negative control, respectively.

PEUU nanofibrous mats and PEUU-NH_2 nanofibrous mats. The PEUU-NH_2 nanofibrous mats experienced more platelet adhesion than PEUU nanofibrous mats, an effect that might be explained by the increased cationic nature of the amine containing polymer [29]. This would be consistent with previous reports on amino-bearing surfaces being associated with increased protein adsorption [29,42]. Endothelial cells (ECs) possess the properties of antiplatelet [48]. In vitro studies also reported positive impact of the RGD to promote attachment and retention of ECs [49]. Thus the rapid endothelialization is a prerequisite for a successful antiplatelet adhesion. The presence of RGD peptide can inhibit platelet adhesion and aggregation. This result can be supported by the former report where the electrospun tubular PCL grafts exhibited an improved inhibition of platelet adhesionwere functionally modified by a RGD-containing molecule through selfresembling [7]. On the other hand, RGD is a peptide with a characteristic sequence of fibronectin, and it can bind to nearly half of all known human

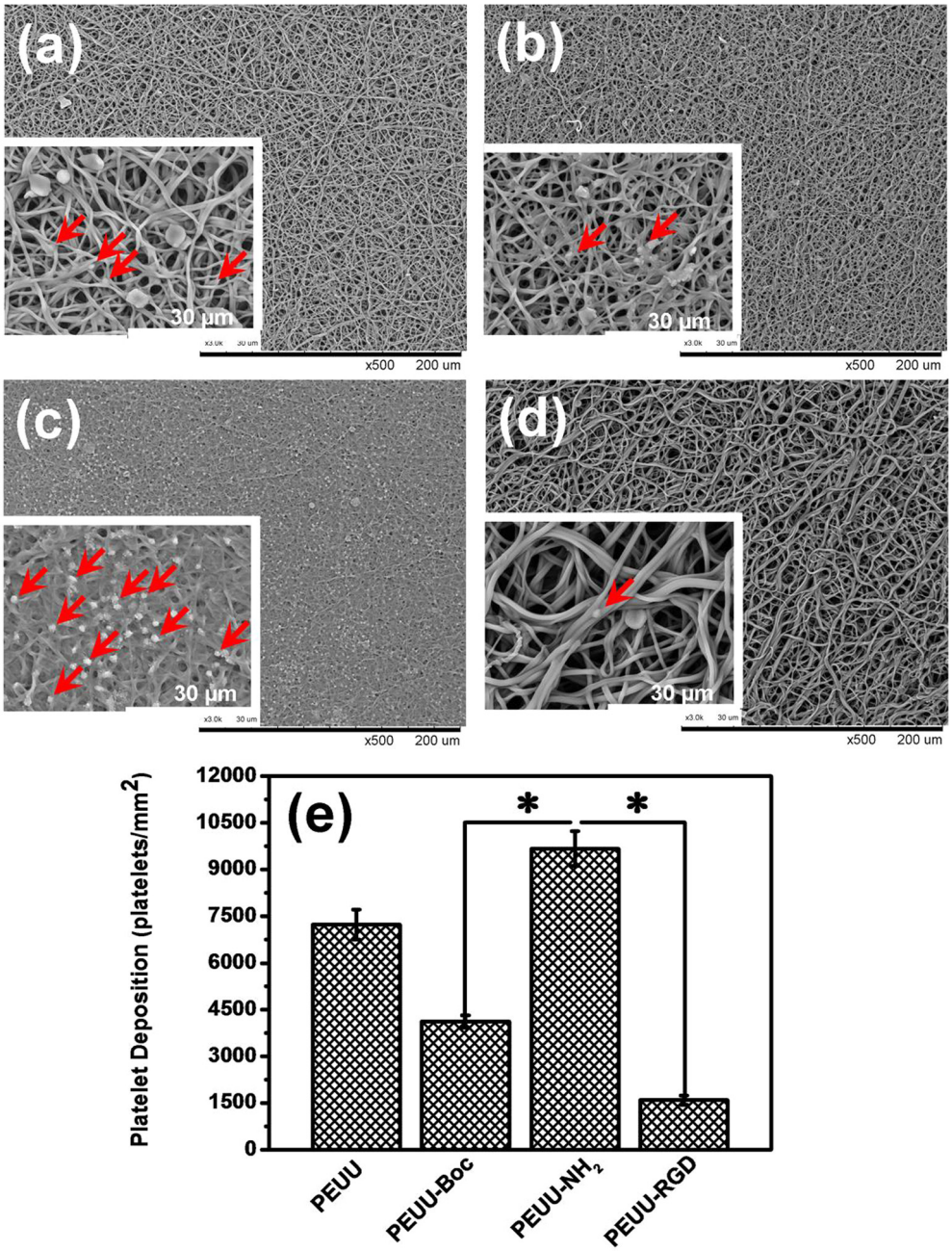

Fig. 11. Effect of grafted RGD on platelet adhesion (3 h contact with rabbit blood): SEM images platelet-rich blood adhesion on PEUU nanofibrous mats (a), PEUU-Boc nanofibrous mats (b), PEUU-NH_2 nanofibrous mats (c), and PEUU-RGD nanofibrous mats (d), as indicated by red arrows; quantification of lactate dehydrogenase activity among four groups (e). (For interpretation of the references to color in this figure legend, the reader is referred to the web version of this article.)

integrins [50]. Adamson et al. designed a monolayer modified gold surfaces with RGD peptide to capture and activation of human platelets and confirmed that platelet adhesion at RGD surfaces is occurring through integrin-RGD interactions [51].

4. Conclusion

In present study, we developed RGD-peptide modified electrospun poly(ester-urethane) urea polymer nanofibrous mats via electrospinning technique and covalent grafting method and characterized by chemical structures analysis. The nanofibrous mats were assessed via mechanical and thermal properties, cell compatibility, and hemocompatibility to evaluate effectiveness as prospective intima for promoting vascular tissue development in situ. The PEUU-RGD nanofibrous mats exhibited a combination of excellent mechanical property, high biocompatibility, and improved inhibition of platelet adhesion. These results suggest that the as-prepared PEUU-RGD nanofibrous mats may be a promising intima for vascular tissue engineering.

Acknowledgements

The authors sincerely appreciate the supports of "National Major Research Program of China (2016YFC1100200)", "National Nature Science Foundation (31470941, 31271035)", "Ph.D Programs Foundation of Ministry of Education of China (20130075110005)". "Science and Technology Commission of Shanghai Municipality of China (15JC1490100, 15441905100)",

"Yantai Double Hundred Talent Plan", and light of textile project (J201404). The authors extend their appreciation to International Scientific Partnership Program ISPP at King Saud University for its funding research through (ISPP-0049).

References

[1] X.K. Ren, Y.K. Feng, J.T. Guo, H.X. Wang, Q. Li, J. Yang, X.F. Hao, J. Lv, N. Ma, W.Z. Li, Surface modification and endothelialization of biomaterials as potential scaffolds for vascular tissue engineering applications, Chem. Soc. Rev. 44 (2015) 5680–5742.

[2] M.A. Cleary, E. Geiger, C. Grady, C. Best, Y.J. Naito, C. Breuer, Vascular tissue engineering: the next generation, Trends Mol. Med. 18 (2012) 394–404.

[3] H.-Y. Mi, X. Jing, E. Yu, J.M. Nulty, X.F. Peng, L.S. Turng, Fabrication of triple-layered vascular scaffolds by combining electrospinning, braiding, and thermally induced phase separation, Mater. Lett. 161 (2015) 305–308.

[4] S.A. Sell, G.L. Bowlin, Creating small diameter bioresorbable vascular grafts through electrospinning, J. Mater. Chem. 18 (2008) 260–263.

[5] G.X. Zhao, X.H. Zhang, T.J. Lu, F. Xu, Recent advances in electrospun nanofibrous scaffolds for cardiac tissue engineering, Adv. Funct. Mater. 25 (2015) 5726–5738.

[6] T. Jiang, E.J. Carbone, K.W.-H. Lo, C.T. Laurencin, Electrospinning of polymer nanofibers for tissue regeneration, Prog. Polym. Sci. 46 (2015) 1–24.

[7] W.T. Zheng, Z.H. Wang, L.S. Song, Q. Zhao, J. Zhang, D. Li, S.F. Wang, J.H. Han, X. L. Zheng, Z.M. Yang, D.L. Kong, Endothelialization and patency of RGD-functionalized vascular grafts in a rabbit carotid artery model, Biomaterials 33 (2012) 2880–2891.

[8] Q. Li, Z.H. Wang, S. Zhang, W.T. Zheng, Q. Zhao, J. Zhang, L.Y. Wang, S.F. Wang, D.L. Kong, Functionalization of the surface of electrospun poly(epsilon-caprolactone) mats using zwitterionic poly(carboxybetaine methacrylate) and cell-specific peptide for endothelial progenitor cells capture, Mater. Sci. Eng. C Mater. 33 (2013) 1646–1653.

[9] Y.Y. Wang, S.Y. Chen, Y.W. Pan, J.C. Gao, D. Tang, D.L. Kong, S.F. Wang, Rapid in situ endothelialization of a small diameter vascular graft with catalytic nitric oxide generation and promoted endothelial cell adhesion, J. Mater. Chem. B 3 (2015) 9212–9222.

[10] G.-H. Yang, F. Mun, G.H. Kim, Direct electrospinning writing for producing 3D hybrid constructs consisting of microfibers and macro-struts for tissue engineering, Chem. Eng. J. 288 (2016) 648–658.

[11] N. Isayama, G. Matsumura, H. Sato, S. Matsuda, K. Yamazaki, Histological maturation of vascular smooth muscle cells in situ tissue-engineered vasculature, Biomaterials 35 (2014) 3589–3595.

[12] Y. Shirosaki, T. Okayama, K. Tsuru, S. Hayakawa, A. Osaka, Synthesis and cytocompatibility of porous chitosan-silicate hybrids for tissue engineering scaffold application, Chem. Eng. J. 137 (2008) 122–128.

[13] H.Y. Wang, Y.K. Feng, B. An, W.C. Zhang, M.L. Sun, Z.C. Fang, W.J. Yuan, M. Khan, Fabrication of PU/PEGMA crosslinked hybrid scaffolds by in situ UV photopolymerization favoring human endothelial cells growth for vascular tissue engineering, J. Mater. Sci. Mater. M 23 (2012) 1499–1510.

[14] T. Yokota, H. Ichikawa, G. Matsumiya, T. Kuratani, T. Sakaguchi, S. Iwai, Y. Shirakawa, K. Torikai, A. Saito, E. Uchimura, In situ tissue regeneration using a novel tissue-engineered, small-caliber vascular graft without cell seeding, J. Thorac. Cardiovasc. Surg. 136 (2008) 900–907.

[15] J.H. Li, M.M. Ding, Q. Fu, H. Tan, X.Y. Xie, Y.P. Zhong, A novel strategy to graft RGD peptide on biomaterials surfaces for endothelization of small-diameter vascular grafts and tissue engineering blood vessel, J. Mater. Sci. Mater. M 19 (2008) 2595–2603.

[16] S.J. Kim, D.H. Jang, W.H. Park, B.-M. Min, Fabrication and characterization of 3-dimensional PLGA nanofiber/microfiber composite scaffolds, Polymer 51 (2010) 1320–1327.

[17] S.J. Peng, G.R. Jin, L.L. Li, K. Li, M. Srinivasan, S. Ramakrishna, J. Chen, Multi-functional electrospun nanofibers for advances in tissue regeneration, energy conversion & storage, and water treatment, Chem. Soc. Rev. 45 (2016) 1225–1241.

[18] H.R. Pant, P. Risal, C.H. Park, L.D. Tijing, Y.J. Jeong, C.S. Kim, Core-shell structured electrospun biomimetic composite nanofibers of calcium lactate/nylon-6 for tissue engineering, Chem. Eng. J. 221 (2013) 90–98.

[19] C.M. Vaz, T.S. Van, C.V.C. Bouten, F.P.T. Baaijens, Design of scaffolds for blood vessel tissue engineering using a multi-layering electrospinning technique, Acta Biomater. 1 (2005) 575–582.

[20] W.G. Cui, Y. Zhou, J. Chang, Electrospun nanofibrous materials for tissue engineering and drug delivery, Sci. Technol. Adv. Mater. 11 (2010) 014108.

[21] T. Subbiah, G.S. Bhat, R.W. Tock, S. Pararneswaran, S.S. Ramkumar, Electrospinning of nanofibers, J. Appl. Polym. Sci. 96 (2005) 557–569.

[22] Z.W. Ma, W. He, T. Yong, S. Ramakrishna, Grafting of gelatin on electrospun poly(caprolactone) nanofibers to improve endothelial cell spreading and proliferation and to control cell orientation, Tissue Eng. 11 (2005) 1149–1158.

[23] J.M. Aamodt, D.W. Grainger, Extracellular matrix-based biomaterial scaffolds and the host response, Biomaterials 86 (2016) 68–82.

[24] R.J. Wade, J.A. Burdick, Advances in nanofibrous scaffolds for biomedical applications: from electrospinning to self-assembly, Nano Today 9 (2014) 722–742.

[25] H. Bergmeister, N. Seyidova, C. Schreiber, M. Strobl, C. Grasl, I. Walter, B. Messner, S. Baudis, S. Fröhlich, M. Marchetti-Deschmann, M. Griesser, M.D. Franco, M. Krssak, R. Liska, H. Schima, Biodegradable, thermoplastic polyurethane grafts for small diameter vascular replacements, Acta Biomater. 11 (2015) 104–113.

[26] E.S. Jamadi, L. Ghasemi-Mobarakeh, M. Morshed, M. Sadeghi, M.P. Prabhakaran, S. Ramakrishna, Synthesis of polyester urethane urea and fabrication of elastomeric nanofibrous scaffolds for myocardial regeneration, Mater. Sci. Eng. C Mater. 63 (2016) 106–116.

[27] P. Punnakitikashem, D. Truong, J.U. Menon, K.T. Nguyen, Y. Hong, Electrospun biodegradable elastic polyurethane scaffolds with dipyridamole release for small diameter vascular grafts, Acta Biomater. 10 (2014) 4618–4628.

[28] J. Fang, S.-H. Ye, J. Wang, T. Zhao, X.M. Mo, W.R. Wanger, Thiol click modification of cyclic disulfide containing biodegradable polyurethane urea elastomers, Biomacromolecules 16 (2015) 1622–1633.

[29] J. Fang, S.-H. Ye, V. Shankarraman, Y.X. Huang, X.M. Mo, W.R. Wanger, Biodegradable poly(ester urethane)urea elastomers with variable amino content for subsequent functionalization with phosphorylcholine, Acta Biomater. 10 (2014) 4639–4649.

[30] W.Z. Wang, J.W. Hu, C.L. He, W. Nie, W. Feng, K.X. Qiu, X.J. Zhou, Y. Gao, G.Q. Wang, Heparinized PLLA/PLCL nanofibrous scaffold for potential engineering of small-diameter blood vessel: Tunable elasticity and anticoagulation property, J. Biomed. Mater. Res. Part A 103A (2015) 1784–1797.

[31] F.Y. Zheng, S.G. Wang, S.H. Wen, M.W. Shen, M.F. Zhu, X.Y. Shi, Characterization and antibacterial activity of amoxicillin-loaded electrospun nano-hydroxyapatite/poly(lactic-co-glycolic acid) composite nanofibers, Biomaterials 34 (2013) 1402–1412.

[32] K.X. Qiu, C.L. He, W. Feng, W.Z. Wang, X.J. Zhou, Z.Q. Yin, L. Chen, H.S. Wang, X. M. Mo, Doxorubicin-loaded electrospun poly(L-lactic acid)/mesoporous silica nanoparticles composite nanofibers for potential postsurgical cancer treatment, J. Mater. Chem. B 1 (2013) 4601–4611.

[33] Y. Hong, A. Huber, K. Takanari, N.J. Amoroso, R. Hashizume, S.F. Badylak, W.R. Wanger, Mechanical properties and in vivo behavior of a biodegradable synthetic polymer microfiber-extracellular matrix hydrogel biohybrid scaffold, Biomaterials 32 (2011) 3387–3394.

[34] C. Carrizales, S. Pelfrey, R. Rincon, T.M. Eubanks, A. Kuang, M.J. McClure, G.L. Bowlin, J. Macossay, Thermal and mechanical properties of electrospun PMMA, PVC, Nylon6 and Nylon 6,6, Polym. Adv. Technol. 19 (2008) 124–130.

[35] J. Fang, J.L. Zhang, J. Du, Y.J. Pan, J. Shi, Y.X. Peng, W.M. Cheng, L. Yuan, S.-H. Ye, W.R. Wagner, M. Yin, X.M. Mo, Orthogonally functionalizable polyurethane with subsequent modification with heparin and endothelium-inducing peptide aiming for vascular reconstruction, ACS Appl. Mater. Interfaces 8 (2016) 14442–14452.

[36] L.-C. Su, H. Xu, R.T. Tran, Y.-T. Tsai, L.P. Tang, S. Banerjee, J. Yang, K.T. Nguyen, In situ re-endothelialization via multifunctional nanoscaffolds, ACS Nano 8 (2014) 10826–10836.

[37] C.W. McCarthy, D.C. Ahrens, D. Joda, T.E. Curtis, P.K. Bowen, R.J. GuilloryII, S.Q. Liu, F. Zhao, M.C. Frost, J. Goldman, Fabrication and short-term in vivo performance of a natural elastic lamina-polymeric hybrid vascular graft, ACS Appl. Mater. Interfaces 7 (2015) 16202–16212.

[38] U. Hersel, C. Dahmen, H. Kessler, RGD modified polymers: biomaterials for stimulated cell adhesion and beyond, Biomaterials 24 (2003) 4385–4415.

[39] Y. Hong, S.H. Ye, A.L. Pelinescu, W.R. Wagner, Synthesis, characterization, and paclitaxel release from a biodegradable, elastomeric, poly(ester urethane)urea bearing phosphorylcholine groups for reduced thrombogenicity, Biomacromolecules 13 (2012) 3686–3694.

[40] Y.C. Shin, J.H. Lee, L. Jin, M.J. Kim, C. Kim, S.W. Hong, J.W. Oh, D.W. Han, Cell-adhesive matrices composed of RGD peptide-displaying M13 bacteriophage/poly(lactic-co-glycolic acid) nanofibers beneficial to myoblast differentiation, J. Nanosci. Nanotechnol. 15 (2015) 7907–7912.

[41] K.N. Chua, C. Chai, P.C. Lee, Y.N. Tang, S. Ramakrishna, K.W. Leong, H.Q. Mao, Surface-aminated electrospun nanofibers enhance adhesion and expansion of human umbilical cord blood hematopoietic stem/progenitor cells, Biomaterials 27 (2006) 6043–6051.

[42] J.J. Guan, M.S. Sacks, E.J. Beckman, W.R. Wanger, Synthesis, characterization and cytocompatibility of efastomeric, biodegradable poly(ester-urethane) ureas based on poly(caprolactone) and putrescine, J. Biomed. Mater. Res. A 61 (2002) 493–503.

[43] D.A. Barrera, E. Zylstra, P.T. Lansbury Jr., R. Langer, Synthesis and RGD peptide modification of a new biodegradable copolymer: poly(lactic acid-co-lysine), J. Am. Chem. Soc. 115 (1993) 11010–11011.

[44] J. Zhao, H. Qiu, D.L. Chen, W.X. Zhang, D.C. Zhang, M. Li, Development of nanofibrous scaffolds for vascular tissue engineering, Int. J. Biol. Macromol. 56 (2013) 106–113.

[45] J.J. Yoon, S.H. Song, D.S. Lee, T.G. Park, Immobilization of cell adhesive RGD peptide onto the surface of highly porous biodegradable polymerscaffolds fabricated by a gas foaming/salt leaching method, Biomaterials 25 (2004) 5613–5620.

[46] Q. Wang, M. Shen, T. Zhao, Y.Y. Xu, J.A. Lin, Y.R. Duan, H.C. Gu, Low toxicity and long circulation time of polyampholyte-coated magnetic nanoparticles for blood pool contrast agents, Sci. Rep. 5 (2015) 7774.

[47] X. Shen, J. Liu, X. Feng, Y.P. Zhao, L. Chen, Preliminary investigation on hemocompatibility of poly(vinylidene fluoride) membrane grafted with acryloylmorpholine via ATRP, J. Biomed. Mater. Res. Part A 103A (2015) 683–692.

[48] D.B. Cines, E.S. Pollak, C.A. Buck, J. Loscalzo, G.A. Zimmerman, R.P. McEver, J.S. Pober, T.M. Wick, B.A. Konkle, B.S. Schwartz, E.S. Barnathan, K.R. McCrae, B.A.

Hug, A.-M. Schmidt, D.M. Stern, Endothelial cells in physiology and in the pathophysiology of vascular disorders, Blood 91 (1998) 3527–3561.
[49] S. Tugulua, P. Silacci, N. Stergiopulos, H.-A. Klok, RGD-Functionalized polymer brushes as substrates for the integrin specific adhesion of human umbilical vein endothelial cells, Biomaterials 28 (2007) 2536–2546.
[50] S.R. Meyers, D.J. Kenan, X. Khoo, M.W. Grinstaff, Bioactive stent surface coating that promotes endothelialization while preventing platelet adhesion, Biomacromolecules 12 (2011) 533–539.
[51] K. Adamson, E. Spain, U. Prendergast, R.J. Forster, N. Moran, T.E. Keyes, Ligand capture and activation of human platelets at monolayer modified gold surfaces, Biomater. Sci. 2 (2014) 1509–1520.